THE JOURNAL OF PHYSICAL CHEMISTRY C

Article

Cite This: J. Phys. Chem. C 2018, 122, 15421−15426

pubs.acs.org/JPCC

Hydrogen Bubble Formation at Hydrogen-Insertion Electrodes

Qianjin Chen,[†,‡] Ruchiranga Ranaweera,[‡] and Long Luo*[,‡]

[†]College of Chemistry, Chemical Engineering and Biotechnology, Donghua University, Shanghai 201620, China

[‡]Department of Chemistry, Wayne State University, Detroit, Michigan 48202, United States

Supporting Information

ABSTRACT: Here we report a fundamental study of the H_2 bubble formation mechanism on a model hydrogen-insertion material, Pd. We demonstrated that the current required for H_2 bubble formation at Pd electrodes was over 10 times higher than that at nonhydrogen-insertion metal electrodes (Au and Pt). Using a newly developed nanoelectrode platform, we measured the critical condition for H_2 bubble formation on different electrode materials. We discovered, for the first time, that the bubble formation on Pd required nearly the same supersaturation of dissolved H_2 on the electrode surface as Au and Pt. The suppressed bubble generation on Pd relative to Au and Pt is caused merely by the hydrogen insertion into bulk Pd rather than the different surface energies of electrode materials. Our study provides new insights into the nanoscale H_2 bubble generation mechanism on hydrogen-insertion materials.

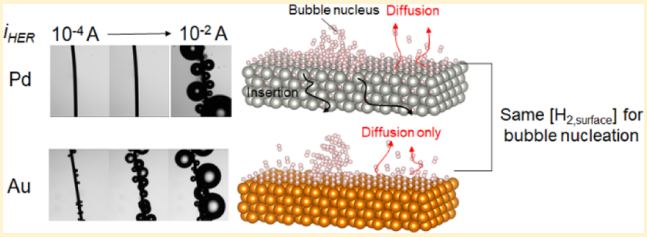

INTRODUCTION

Electrolytic gas evolution is a significant phenomenon in many electrochemical processes and devices.[1,2] These include water splitting,[3] chlor-alkali process,[4] lead acid batteries,[5] Ni-metal hydride batteries,[6,7] metal electrowinning,[8] the Hall process for aluminum production,[9] chlorate production,[10] and so forth. Gas evolution process may substantially affect the ohmic resistance of the electrolyte as well as the heat and mass transfer in these electrochemical systems. To improve the efficiency of these systems, it is essential to understand the electrolytic gas evolution process. Gas evolution is a dynamic phenomenon that is closely related with the potential, electrode material, and electrolyte solution. The dynamics of gas bubbles on electrode surfaces has been widely studied using a variety of technologies including high-speed photography,[11−13] in situ transmission electron microscopy,[14,15] atomic force microscopy,[16,17] and so forth. Recently, single-molecule fluorescence microscopy[18,19] and dark field microscopy[20] have also been used for studying the dynamics of nanosized bubbles associated with single-nanoparticle catalytic activity. Despite the above progress, the accurate measurement of the nucleation condition for bubbles is still challenging. Most recently, an electrochemical method developed by the White group and us overcomes this challenge.[21−25] This method employs nanoelectrodes (NEs) that have comparable sizes to gas bubble nuclei for detecting gas bubble nucleation. Using this method, the critical condition for H_2 gas bubble formation at Pt NEs has been measured to be ∼300-fold supersaturation of dissolved H_2 and the critical nucleus size to be 4.4 to 5.3 nm.[25] More interestingly, we recently discovered that H_2 gas bubble formation at Au and Pt NEs required a very similar supersaturation of dissolved H_2 even though they exhibit significantly different activities for the hydrogen evolution reaction (HER).[26] Here, we extend our study to another common HER electrocatalytic material, Pd, where the hydrogen insertion takes place during the HER. We discovered that the H_2 bubble formation at Pd NEs required more than 10 times higher current density than that at the Pt and Au NEs. The suppression of bubble generation on Pd is merely caused by the hydrogen insertion into the Pd bulk.

EXPERIMENTAL SECTION

Chemicals and Materials. Perchloric acid ($HClO_4$, 70%), sulfuric acid (H_2SO_4, 95−98%), sodium perchlorate ($NaClO_4$, 98%), potassium chloride (KCl, 99%), anhydrous copper(II) sulfate ($CuSO_4$, 99%), potassium tetrachloropalladate(II) (K_2PdCl_4, 99.99%), hexaammineruthenium(III) chloride ($Ru(NH_3)_6Cl_3$, 98%), and calcium chloride ($CaCl_2$, 99%) were all purchased from Sigma-Aldrich. The glass capillary (o.d./i.d.,1.65/1.10 mm, soft temperature, 785 °C) was received from Dagan Corporation. Platinum (Pt, 25 and 50 μm diameter, 99.95%), gold (Au, 25 and 50 μm diameter, 99.95%), and palladium (Pd, 50 μm diameter, 99.9%) wires were purchased from Alfa Aesar. Silver conductive epoxy was purchased from MG Chemicals. All aqueous solutions were prepared from deionized (DI) water (PURELAB, 18.2 MΩ/cm, TOC < 3 ppb).

Electrochemical Measurements. All electrochemical experiments were completed using a CHI 760E potentiostat and inside a well-grounded Faraday cage. For electrochemistry at NEs, an Ag/AgCl electrode in saturated KCl was used as the

Received: April 21, 2018
Revised: June 3, 2018
Published: June 13, 2018

DOI: 10.1021/acs.jpcc.8b03770
J. Phys. Chem. C 2018, 122, 15421−15426

counter/reference electrode. To avoid the undesired Pd electrooxidation, the potential of Pd NEs during the electrochemical measurement was kept between 0 and −1.2 V versus Ag/AgCl. For the bubble formation at wire electrodes, a 50 μm diameter Pd, Pt, or Au wire was used as the working electrode and a 1 mm diameter Pt wire as the counter. The working electrodes were immersed 1.0 cm into 1.0 M $HClO_4$ solution, and the chronopotentiometric measurements were carried out by applying a constant current from 10^{-5} to 10^{-2} A, 10 s for each current level.

Fabrication of Pt, Au, and Pd NEs. Pt, Au, and Pd NEs were fabricated based on a method previously reported with necessary modifications.[27] The procedures are depicted in Figure S1. Briefly, the end of a 25 μm diameter Pt or Au wire or 50 μm diameter Pd wire was attached to a tungsten rod using silver conductive epoxy. The tips were electrochemically sharpened in 15 wt % $CaCl_2$ solution using different waveforms (sinusoidal wave with 100 Hz frequency and V_{app} = 4.0 V for Pt; sinusoidal wave with 100 Hz frequency and V_{app} = 4.8 V for Au; and pulse wave with 100 Hz frequency and V_{app} = 2.5 V, V_{offset} = 1.25 V for Pd, respectively). After etching, the Pt and Au tips were cleaned by rinsing in DI water. The Pd tips were sequentially dipped into a dilute HCl solution, a KCl solution, and DI water to remove the $PdCl_2$ layer formed during the etching. Scanning electron microscopy (SEM) images for the resulting sharpened tips are shown in Figure S2. The radii of curvature are ~25 nm. During the thermal sealing of the Pd nanotip inside a glass capillary, an Ar flow was applied to prevent the thermal oxidation of Pd, whereas for Pt or Au, the thermal sealing was completed directly in the air. Finally, the glass capillary containing a nanotip was polished on a silicon carbide sandpaper (400/4000 grit, Buehler) until a nanodisk was exposed, as monitored by an electronic feedback circuit. The electrode radius, r, was electrochemically determined by measuring the diffusion-limited current for proton reduction in 0.10 M $HClO_4$.

Fabrication of Au@Pd NEs. Preparation of an Au@Pd NE was carried out by underpotential deposition of a monolayer of Cu onto an Au NE at 0.12 V versus Ag/AgCl in a solution of 0.1 M H_2SO_4 containing 5.0 mM $CuSO_4$.[28,29] Following the successful deposition of Cu, 0.1 mL of 0.2 mg/mL K_2PdCl_4 was added to the solution for the galvanic exchange with Cu. This process was completed in 1 min as indicated by a shift of open-circuit potential of the NE to a potential plateau.

RESULTS AND DISCUSSION

H_2 Bubble Formation on Wire Electrodes. Figure 1a–c shows the photographs of 50 μm diameter and 1 cm long Pd, Pt, and Au wire electrodes that were immersed in 1.0 M $HClO_4$ at various applied currents. Au and Pt were employed as the negative controls because they are known to absorb hydrogen barely.[30−32] In this experiment, the current was stepped from 10^{-5} to 10^{-2} A with a step size of 10-fold increase and a duration time of 10 s at each current level (the corresponding videos are provided in the Supporting Information Video S1). For Pd, H_2 gas bubbles began to appear on the wire immediately after a current of 10^{-2} A was applied. Meanwhile, the twist motion of the Pd wire was observed (see Video S2). The current-triggered physical motion is caused by the structural swelling of the Pd wire due to the absorption and interstitial introduction of hydrogen atoms into the Pd lattice.[33,34] We further investigated the condition for H_2 bubble formation on the Pd wire by

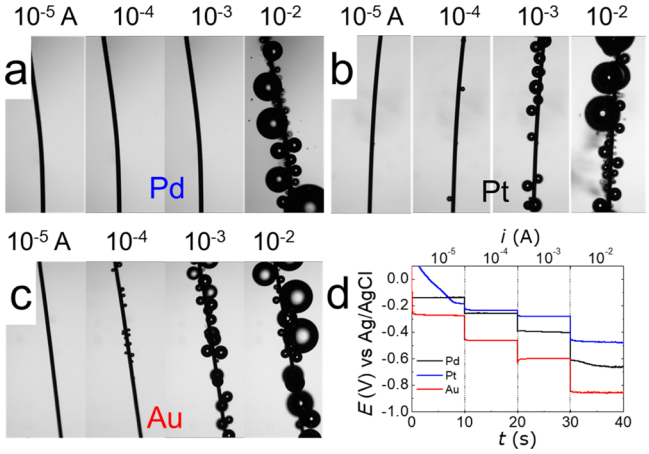

Figure 1. Photographs of the hydrogen bubble formation at 50 μm diameter and 1.0 cm long (a) Pd, (b) Pt, and (c) Au wire electrodes immersed in 1.0 M $HClO_4$ at the current levels as labeled. H_2 gas bubbles started forming at 10^{-2} A for the Pd electrode, whereas for Pt and Au electrodes, H_2 gas bubbles started forming at 10^{-4} A. The experiments were carried out by sequentially stepping the current from 10^{-5} to 10^{-2} A every 10 s. The corresponding potential−time (E−t) traces are shown in (d) and the videos are provided in the supporting information Video S1.

estimating the degree of hydrogen insertion. At E < −0.2 V versus Ag/AgCl and room temperature, the thermodynamically stable phase of palladium hydride is the β-phase with the H/Pd ratio of ~0.75.[35] Accordingly, the H-absorption capacity for the Pd wire is ~1.6 μmol H atoms or 0.16 C. This value is more than the total charge supplied during the entire current step experiment (~0.11 C), suggesting that the H_2 bubbles start forming before the hydrogen insertion is complete. Similar experiments were carried out using Pt and Au wire electrodes with the identical dimensions. For both electrodes, H_2 gas bubble formation was found at 10^{-4} A and no apparent physical motion was observed.

The potential−time (E−t) traces were recorded throughout the current step experiments as shown in Figure 1d. For all three wire electrodes, the electrode potential stayed relatively constant at applied currents >10^{-4} A. The negative drift of E for Pt at 10^{-5} A is due to the concentration polarization from the oxygen reduction reaction. The potential magnitude in the E−t traces for Pd, Pt, and Au is consistent with their relative HER activities.[36]

The above result clearly demonstrates that the Pd wire electrode requires over 10 times higher current than Pt and Au electrodes to form H_2 bubbles. There are several possible reasons that account for the required higher current. The most likely one is the hydrogen insertion into Pd electrodes. Because electrogenerated hydrogen is partially consumed by the insertion into Pd, the concentration of dissolved H_2 near a Pd electrode is thus lower than that near a Pt or Au electrode at the same applied current. Therefore, a higher current might be required to nucleate bubbles at Pd electrodes. Alternatively, it is also possible that the observed bubble-forming behaviors are caused by the inherently different surface energies of Pd, Pt, and Au. According to the classical heterogeneous nucleation theory, the rate of gas bubble nucleation on a surface is a function of the free energies of the gas/metal and liquid/metal interfaces.[25,37]

Single H_2 Nanobubble Formation at Pd NEs. To clearly disentangle the two possible mechanisms described above, we

DOI: 10.1021/acs.jpcc.8b03770
J. Phys. Chem. C 2018, 122, 15421−15426

directly measure the critical concentration of dissolved H_2 required for bubble formation ($C_{critical}$) at Pd, Pt, and Au electrodes by conducting a single nanobubble study. If Pd, Pt, and Au electrodes have the same $C_{critical}$, the first mechanism is correct. Otherwise, the second mechanism should also be playing an important role.

The single nanobubble study was carried out by fabricating Pd, Pt, and Au NEs using a modified method that has been previously reported (see Supporting Information and Figures S1 and S2).[27,38] After being fabricated, the NEs have been characterized by SEM (Figure S3). The apparent radii were estimated from the steady-state voltammograms for proton reduction in 0.1 M $HClO_4$ solution with 0.2 M $NaClO_4$ (Figure S4). In addition, the voltammograms of NEs in a 0.1 M NaCl solution containing 25 mM $Ru(NH_3)_6^{3+}$ show no indication of redox peaks at a high scan rate of 4 V/s (Figure S5), suggesting that the NEs were well sealed and had no significant solution leakage after preparation.[39,40]

Figure 2 shows the typical voltammograms for the prepared Pd, Pt, and Au NEs with similar sizes (radii of ~20 nm) in N_2-purged 1.0 M $HClO_4$. For all three NEs, we observed the peak-shaped voltammetric response in the forward scans, which is the characteristic feature for the nucleation and formation of a single gas nanobubble at an NE (Figure 2a–c). The gas nanobubble nucleates at the peak current (i_{nb}) where $C_{critical}$ is reached. The subsequent formation of a gas nanobubble physically blocks the NE surface leading to a ~90% drop in current. Consistent with the previous finding for bubble nucleation at Pt NE,[21] i_{nb} at Pd and Au NEs changes less than 15% with a 10-fold change in the scan rate (Figure 2d–f). It indicates that the diffusion of H^+ and electrogenerated H_2 at the NEs is at steady state when a bubble nucleates and forms.

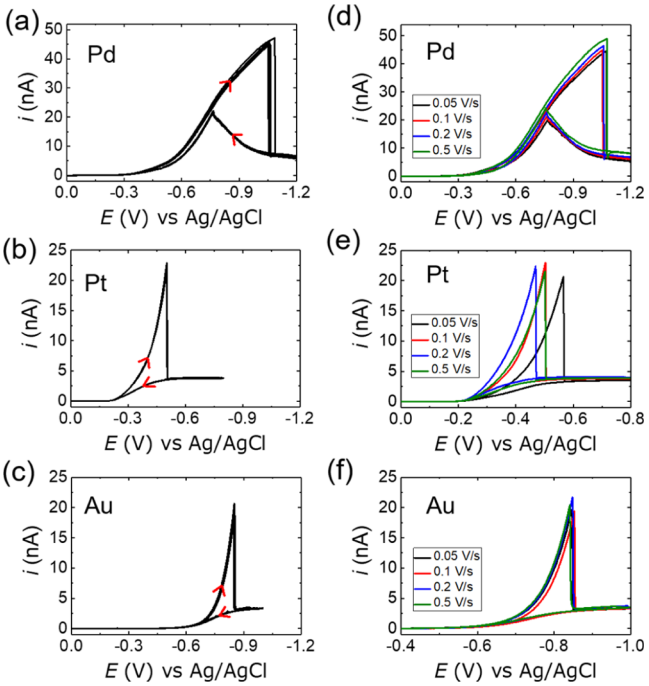

Figure 2. Cyclic voltammograms of (a) 18 nm radius Pd, (b) 20 nm radius Pt, and (c) 19 nm radius Au NEs in N_2-purged 1.0 M $HClO_4$ for three potential cycles within the range as labeled vs Ag/AgCl at a scan rate of 100.0 mV/s. (d–f) Cyclic voltammograms of the same electrodes at scan rates of 50, 100, 200, and 500 mV/s.

Also, note that although the Pt NE in Figure 2 shows a more significant variation of the bubble formation potential at various scan rates than the Pd and Au counterparts, we found that such a variation was not constant after testing multiple Pt NEs.

At steady state, $C_{critical}$ for nonhydrogen-insertion materials, such as Pt and Au, can be directly estimated from the ratio of i_{nb}/r by[24]

$$C_{critical} = \frac{i_{nb}}{4nFD_{H_2}r} \quad (1)$$

where D_{H_2} is the diffusivity of H_2 in water (4.5×10^{-5} cm^2/s), n is the number of electron transfer per H_2 ($n = 2$), F is the Faraday's constant, and r is the apparent electrode radius. In Figure 3, Au and Pt NEs show similar values of i_{nb}/r: 1.1 and

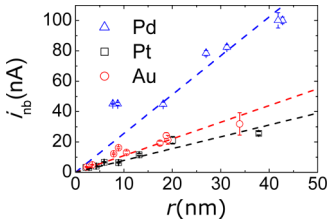

Figure 3. Peak current (i_{nb}) of the cyclic voltammograms for Pd, Pt, and Au NEs in N_2-purged 1.0 M $HClO_4$ vs NE radii (r). Error bars are from at least three independent measurements using the same electrode. The dashed lines are the best linear fits of the data.

0.9 A/m, respectively. Their $C_{critical}$ values were then calculated to be 0.32 and 0.26 M, respectively, which are about 300- to 400-fold supersaturation of dissolved H_2 in water at ambient conditions (0.78 mM). For Pd NEs, however, eq 1 is no longer valid because it assumes that all of the electrogenerated hydrogen diffuses into the aqueous solution.

Single H_2 Nanobubble Formation at Au@Pd NEs. To figure out $C_{critical}$ for Pd NEs, we performed a control experiment using an Au NE modified by a monolayer of Pd (Au@Pd NE). Our argument is that the Pd monolayer is sufficiently thin that the hydrogen insertion is readily completed prior to the H_2 bubble formation during the potential scan. In other words, the hydrogen-insertion flux is negligible for the Au@Pd NE at i_{nb}. Meanwhile, the Pd monolayer mostly retains the surface properties of pure Pd. Taken together, we can estimate the $C_{critical}$ for Pd NEs from the i_{nb} for the Au@Pd NE using eq 1.

Preparation of an Au@Pd NE was performed by underpotentially depositing a monolayer of Cu onto an Au NE (Au@Cu NE) at 0.12 V versus Ag/AgCl for 20 s in a solution of 0.1 M H_2SO_4 containing 5.0 mM $CuSO_4$ (Figure 4a).[28,29] Following the successful deposition of Cu, 0.1 mL of 0.2 mg/mL K_2PdCl_4 was added to the solution for the galvanic exchange with Cu. This process was completed in 1 min as indicated by the open-circuit potential reaching a plateau. The resulting Au@Pd NE has the same radius as the initial Au NE, suggesting no three-dimensional deposition of Cu (Figure S6). However, we would like to point out that the Cu stripping voltammogram of the 34 nm radius Au@Cu NE in Figure 4b shows a total charge of ~11 pC, which is equivalent to ~500 layers of Cu atoms being deposited at the Au NE. A similar result has been previously reported by Mirkin and co-workers when they underpotentially deposited Cu on Pt NEs.[40] They

DOI: 10.1021/acs.jpcc.8b03770
J. Phys. Chem. C 2018, 122, 15421–15426

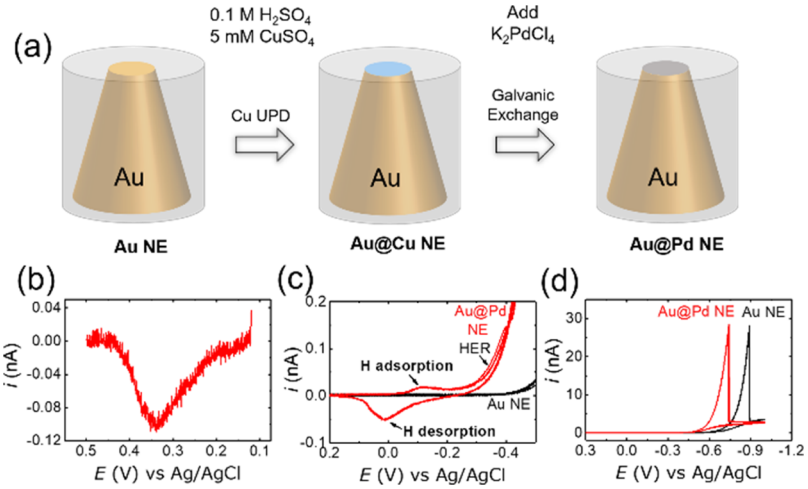

Figure 4. (a) Scheme for preparing an Au NE modified by a monolayer of Pd (Au@Pd NE) via Cu underpotential deposition followed by the galvanic exchange with K_2PdCl_4. (b) Stripping voltammogram for an Au@Cu NE. Cu was underpotentially deposited by holding the potential of a 34 nm radius Au NE at 0.12 V vs Ag/AgCl for 20 s in 0.10 M H_2SO_4 containing 5 mM $CuSO_4$. The potential was then swiped from 0.12 to 0.5 V to oxidize the electrodeposited Cu at a scan rate of 1.0 V/s. (c) Cyclic voltammograms of an Au NE and the resulting Au@Pd NE in 0.10 M H_2SO_4 at a scan rate of 100 mV/s. The Au@Pd and Au NEs have the same electrode radius of 34 nm. (d) Cyclic voltammograms of Au and Au@Pd NEs in 1.0 M $HClO_4$ at a scan rate of 100 mV/s.

attributed it to the additional electrodeposition of Cu along the Pt/glass boundary of the NE (in our case, the Au/glass boundary). Even with the excess deposition of Pd, the amount of Pd in the Au@Pd NE is still incomparably smaller ($\sim 5 \times 10^{-17}$ mol) than the amount of H_2 ($\sim 2 \times 10^{-13}$ mol) electrogenerated in our cyclic voltammetry experiment. Therefore, the additional Pd in the Au@Pd NE will not alter the conclusion of this control experiment. In addition, to test the presence of a Pd monolayer at the Au NE, we attempted the SEM/energy-dispersive X-ray spectrometry (EDXS) analysis of Au@Pd NEs. However, it turned out to be very difficult to image NEs with radii < 50 nm because of the severe charge accumulation on the surrounding glass surface from electron exposure. As a result, we used a 1 μm radius Au ultramicroelectrode as an alternative. The SEM images and EDXS results show the presence of <5 weight % Pd on the Au@Pd ultramicroelectrode. Because the signal of Pd is weak, no definitive conclusion of the Pd layer thickness can be drawn. In any events, the SEM/EDXS study suggests that only a small amount of Pd is deposited onto the Au NE using Cu underpotential deposition followed by galvanic exchange.

Figure 4c,d shows the typical voltammetric response of an Au NE and the prepared Au@Pd NE in an acid solution with different potential windows. The pair of peaks at −0.1 and 0 V in Figure 4c corresponds to H adsorption and desorption at the Au@Pd NE in the potential range positive of the onset of bulk H_2 evolution. At more negative potentials, we found the characteristic peak-shaped responses associated with the H_2 bubble formation at both NEs (Figure 4d). The positive shift of the HER onset potential for the Au@Pd NE relative to the Au NE further confirms the successful deposition of Pd. Although the Au@Pd NE shows an HER onset potential (~−0.4 V) similar to that of the Pd NE in Figure 1, their bubble formation potentials are significantly different: −0.75 V versus −1.0 V. Most interestingly, i_{nb} is virtually identical for the Au@Pd and Au NEs. According to eq 1, the same i_{nb} indicates that the Au@Pd and Au NEs have the same $C_{critical}$ for H_2 bubble formation. Taken together, we conclude that the first mechanism discussed earlier is the correct mechanism for bubble formation on Pd. That is, the larger current required for H_2 bubble formation by Pd electrodes relative to Pt and Au electrodes is caused merely by the hydrogen insertion rather than the different surface energies of electrode materials.

Hydrogen Insertion at Pd NEs. After identifying the origin of the high i_{nb} for Pd electrodes, we continue to study the hydrogen insertion at Pd NEs. Assuming the pure diffusion-controlled mechanism, the flux of hydrogen insertion into a Pd NE (J_H) is governed by

$$J_H = -D_H \nabla C_H \tag{2}$$

where D_H and C_H are the hydrogen diffusion constant and hydrogen concentration in Pd, respectively. At $i = i_{nb}$, C_H at the NE surface is 75 M, which is approximately the equivalent concentration of H in the β-phase palladium hydride ($C_{H,PdH}$).[41] J_H can be calculated from the cathodic current by

$$J_H = \frac{1}{F}\frac{d(i_{nb} - i_{nb,sol})}{dA} \tag{3}$$

where $i_{nb,sol}$ is the portion of the total current i_{nb} corresponding to the diffusional flux of H_2 into the solution and A is the NE area. Because Pd and Au NEs have the same $C_{critical}$, $i_{nb,sol}$ for a Pd NE is equal to i_{nb} for an Au NE having the same size. On the basis of eqs 2 and 3, we built a finite element model for H diffusion into a Pd NE and estimated D_H to be 2.4×10^{-6} cm^2/s (see Supporting Information and Figure S8 for simulation details, and the simulated hydrogen distributions in the solution and inside the Pd NE are provided in Figure S9). The value of D_H reported here is a few times larger than the ones obtained from macroscale measurements (2 to 4×10^{-7} cm^2/s).[41−43] The reason for such a discrepancy is currently unclear and it might be the result of nanosize effect.

On the basis of the single nanobubble study, we now set out to quantitatively interpret the phenomenon of suppressed bubble formation on the Pd wire electrode in Figure 1. As concluded above, the bubble formation on Pd, Au, and Pt electrodes requires nearly the same local supersaturation of dissolved H_2 on the surface, and the higher bubble formation current, i_{nb}, for Pd relative to Au and Pt arises from the H

DOI: 10.1021/acs.jpcc.8b03770
J. Phys. Chem. C 2018, 122, 15421−15426

insertion. Thus, the ratio between the bubble formation currents on Pd and Au wires (i_{Pd}/i_{Au}) can be simply given by

$$\frac{i_{Pd}}{i_{Au}} = \frac{i_{diff,sol} + i_{insert}}{i_{diff,sol}} \quad (4)$$

where $i_{diff,sol}$ and i_{insert} are the currents corresponding to the diffusional flux of H_2 into the solution and the flux of H insertion into Pd during bubble formation, respectively. As shown in Figure 1 and Video S1, the bubbles initially formed at a few active surface sites. These sites can be regarded as individual disk nano or microelectrodes with apparent radii of r. Accordingly, $i_{diff,sol}$ and i_{insert} are approximated by the following equations.[44]

$$i_{diff,sol} = 4nFD_{H_2}rC_{critical} \quad (5)$$

$$i_{insert} = 4FD_{H}rC_{H,PdH} \quad (6)$$

Combining 4 and substituting the simulated D_H of 2.4×10^{-6} cm^2/s yield the ratio of i_{Pd}/i_{Au} of ~8, smaller than the experimental value of >10. Given the rough approximations used in this calculation, the calculated value of i_{Pd}/i_{Au} is in reasonably good agreement with the experimental observation.

CONCLUSIONS

In conclusion, we have presented a fundamental study of the H_2 bubble formation on a model hydrogen-insertion material, Pd. We demonstrated Pd electrodes required a much larger current (>10 times) to form H_2 bubbles than nonhydrogen-insertion electrodes such as Pt and Au. On the basis of the results from the single nanobubble experiments, we conclude that the suppressed H_2 bubble generation at Pd electrodes is caused merely by the hydrogen insertion rather than the different surface energies of electrode materials. In fact, we found, for the first time, that H_2 bubbles nucleated at Pd electrodes under the similar critical condition as that at Au and Pt electrodes: 300- to 400-fold supersaturation of dissolved H_2 on the electrode surface. Furthermore, we used these findings to understand the bubble formation behaviors on wire electrodes quantitatively and have achieved reasonably good agreement with experimental observation. The above findings are significant for shedding light on the nanoscale bubble formation process on hydrogen-insertion materials.

ASSOCIATED CONTENT

Supporting Information

The Supporting Information is available free of charge on the ACS Publications website at DOI: 10.1021/acs.jpcc.8b03770.

Details of finite element simulations; schematic for the preparation of NEs; SEM images of NEs; electrochemical estimation of the NE radii; cyclic voltammograms of NEs at different scan rates; and cyclic voltammograms of an Au NE and the prepared Au@Pd NE (DOCX)

H_2 bubble formation in Pt, Au, and Pd NEs at different current levels (AVI)

Twist motion of a Pd wire (AVI)

AUTHOR INFORMATION

Corresponding Author

*E-mail: long.luo@wayne.edu.

ORCID

Long Luo: 0000-0001-5771-6892

Notes

The authors declare no competing financial interest.

ACKNOWLEDGMENTS

This work was supported by the start-up funds and Ebbing Faculty Development Award from Wayne State University. We thank Dr. Kwo Young at BASF Corporation, Dr. Joaquín Rodríguez-López at the University of Illinois at Urbana Champaign, and Dr. Stephanie Brock at Wayne State University for helpful discussions.

REFERENCES

(1) Vogt, H. Gas-evolving electrodes. *Comprehensive Treatise of Electrochemistry*; Springer, 1983; pp 445−489.
(2) Sides, P. J. Phenomena and effects of electrolytic gas evolution. *Modern Aspects of Electrochemistry*; Springer, 1986; pp 303−354.
(3) Zou, Z.; Ye, J.; Sayama, K.; Arakawa, H. Direct splitting of water under visible light irradiation with an oxide semiconductor photocatalyst. *Nature* **2001**, *414*, 625−627.
(4) Karlsson, R. K. B.; Cornell, A. Selectivity between oxygen and chlorine evolution in the chlor-alkali and chlorate processes. *Chem. Rev.* **2016**, *116*, 2982−3028.
(5) Ruetschi, P. Aging mechanisms and service life of lead-acid batteries. *J. Power Sources* **2004**, *127*, 33−44.
(6) Ovshinsky, S. R.; Fetcenko, M. A.; Ross, J. A nickel metal hydride battery for electric vehicles. *Science* **1993**, *260*, 176−181.
(7) Young, K.-h.; Yasuoka, S. Capacity degradation mechanisms in nickel/metal hydride batteries. *Batteries* **2016**, *2*, 3.
(8) Saleh, M. M.; Weidner, J. W.; Ateya, B. G. Electrowinning of Non-Noble Metals with Simultaneous Hydrogen Evolution at Flow-Through Porous Electrodes. *J. Electrochem. Soc.* **1995**, *142*, 4113−4121.
(9) Kvande, H.; Haupin, W. Inert anodes for AI smelters: Energy balances and environmental impact. *JOM* **2001**, *53*, 29−33.
(10) Hardee, K. L. The influence of electrolyte parameters on the percent oxygen evolved from a chlorate cell. *J. Electrochem. Soc.* **1989**, *136*, 3314−3318.
(11) Fernández, D.; Maurer, P.; Martine, M.; Coey, J. M. D.; Möbius, M. E. Bubble formation at a gas-evolving microelectrode. *Langmuir* **2014**, *30*, 13065−13074.
(12) Yang, X.; Karnbach, F.; Uhlemann, M.; Odenbach, S.; Eckert, K. Dynamics of single hydrogen bubbles at a platinum microelectrode. *Langmuir* **2015**, *31*, 8184−8193.
(13) Monzon, L. M. A.; Gillen, A. J.; Mobius, M. E.; Coey, J. M. D. Effect of tetraalkylammonium cations on gas coalescence at a hydrogen-evolving microelectrode. *Langmuir* **2015**, *31*, 5738−5747.
(14) Niu, K.; Frolov, T.; Xin, H. L.; Wang, J.; Asta, M.; Zheng, H. Bubble nucleation and migration in a lead-iron hydr(oxide) core-shell nanoparticle. *Proc. Natl. Acad. Sci. U.S.A.* **2015**, *112*, 12928−12932.
(15) Han, B.; Stoerzinger, K. A.; Tileli, V.; Gamalski, A. D.; Stach, E. A.; Shao-Horn, Y. Nanoscale structural oscillations in perovskite oxides induced by oxygen evolution. *Nat. Mater.* **2017**, *16*, 121−126.
(16) Zhang, X. H.; Khan, A.; Ducker, W. A. A nanoscale gas state. *Phys. Rev. Lett.* **2007**, *98*, 136101.
(17) Borkent, B. M.; Dammer, S. M.; Schönherr, H.; Vancso, G. J.; Lohse, D. Superstability of surface nanobubbles. *Phys. Rev. Lett.* **2007**, *98*, 204502.
(18) Su, H.; Fang, Y.; Chen, F.; Wang, W. Monitoring the dynamic photocatalytic activity of single CdS nanoparticles by lighting up H2 nanobubbles with fluorescent dyes. *Chem. Sci.* **2018**, *9*, 1448−1453.
(19) Hao, R.; Fan, Y.; Howard, M. D.; Vaughan, J. C.; Zhang, B. Imaging nanobubble nucleation and hydrogen spillover during electrocatalytic water splitting. *Proc. Natl. Acad. Sci. U.S.A.* **2018**, *115*, 5878.

DOI: 10.1021/acs.jpcc.8b03770
J. Phys. Chem. C 2018, 122, 15421−15426

(20) Li, S.; Du, Y.; He, T.; Shen, Y.; Bai, C.; Ning, F.; Hu, X.; Wang, W.; Xi, S.; Zhou, X. Nanobubbles: An effective way to study gas-generating catalysis on a single nanoparticle. *J. Am. Chem. Soc.* **2017**, *139*, 14277−14284.
(21) Luo, L.; White, H. S. Electrogeneration of single nanobubbles at sub-50-nm-radius platinum nanodisk electrodes. *Langmuir* **2013**, *29*, 11169−11175.
(22) Ren, H.; German, S. R.; Edwards, M. A.; Chen, Q.; White, H. S. Electrochemical Generation of Individual O2 Nanobubbles via H2O2 Oxidation. *J. Phys. Chem. Lett.* **2017**, *8*, 2450−2454.
(23) Chen, Q.; Wiedenroth, H. S.; German, S. R.; White, H. S. Electrochemical Nucleation of Stable N2 Nanobubbles at Pt Nanoelectrodes. *J. Am. Chem. Soc.* **2015**, *137*, 12064−12069.
(24) Chen, Q.; Luo, L.; Faraji, H.; Feldberg, S. W.; White, H. S. Electrochemical Measurements of Single H2 Nanobubble Nucleation and Stability at Pt Nanoelectrodes. *J. Phys. Chem. Lett.* **2014**, *5*, 3539−3544.
(25) German, S. R.; Edwards, M. A.; Ren, H.; White, H. S. Critical Nuclei Size, Rate, and Activation Energy of H2 Gas Nucleation. *J. Am. Chem. Soc.* **2018**, *140*, 4047−4053.
(26) Chen, Q.; Luo, L. Correlation between gas bubble formation and hydrogen evolution reaction kinetics at nanoelectrodes. *Langmuir* **2018**, *34*, 4554−4559.
(27) Zhang, B.; Galusha, J.; Shiozawa, P. G.; Wang, G.; Bergren, A. J.; Jones, R. M.; White, R. J.; Ervin, E. N.; Cauley, C. C.; White, H. S. Bench-top method for fabricating glass-sealed nanodisk electrodes, glass nanopore electrodes, and glass nanopore membranes of controlled size. *Anal. Chem.* **2007**, *79*, 4778−4787.
(28) Herrero, E.; Buller, L. J.; Abruña, H. D. Underpotential deposition at single crystal surfaces of Au, Pt, Ag and other materials. *Chem. Rev.* **2001**, *101*, 1897−1930.
(29) Luo, L.; Duan, Z.; Li, H.; Kim, J.; Henkelman, G.; Crooks, R. M. Tunability of the adsorbate binding on bimetallic alloy nanoparticles for the optimization of catalytic hydrogenation. *J. Am. Chem. Soc.* **2017**, *139*, 5538−5546.
(30) Maeland, A.; Flanagan, T. B. X-ray and thermodynamic studies of the absorption of hydrogen by gold-palladium alloys. *J. Phys. Chem.* **1965**, *69*, 3575−3581.
(31) Berry, A. J. LVI.-The occlusion of hydrogen by the palladium-gold alloys. *J. Chem. Soc.* **1911**, *99*, 463−466.
(32) Hoare, J. P.; Castellan, G. W.; Schuldiner, S. Potentials of noble metal and palladium alloy hydrogen electrodes. *J. Phys. Chem.* **1958**, *62*, 1141−1142.
(33) Carpena-Núñez, J.; Yang, D.; Kim, J.-W.; Park, C.; Fonseca, L. F. Mechanical characterization of pristine and hydrogen-exposed palladium nanowires byin situTEM. *Nanotechnology* **2012**, *24*, 035701.
(34) Nishi, Y.; Uchida, H.-H.; Honjo, T. High responsiveness induced by palladium deposition on thin film actuator of $LaNi_5$ hydrogen storage alloy. *Mater. Trans.* **2005**, *46*, 126−129.
(35) Łukaszewski, M.; Hubkowska, K.; Czerwiński, A. Electrochemical absorption and oxidation of hydrogen on palladium alloys with platinum, gold and rhodium. *Phys. Chem. Chem. Phys.* **2010**, *12*, 14567−14572.
(36) Greeley, J.; Jaramillo, T. F.; Bonde, J.; Chorkendorff, I.; Nørskov, J. K. Computational high-throughput screening of electrocatalytic materials for hydrogen evolution. *Nat. Mater.* **2006**, *5*, 909−913.
(37) Lubetkin, S.; Blackwell, M. The nucleation of bubbles in supersaturated solutions. *J. Colloid Interface Sci.* **1988**, *126*, 610−615.
(38) Penner, R. M.; Heben, M. J.; Longin, T. L.; Lewis, N. S. Fabrication and use of nanometer-sized electrodes in electrochemistry. *Science* **1990**, *250*, 1118−1121.
(39) Zhang, B.; Zhang, Y.; White, H. S. The nanopore electrode. *Anal. Chem.* **2004**, *76*, 6229−6238.
(40) Zhan, D.; Velmurugan, J.; Mirkin, M. V. Adsorption/desorption of hydrogen on Pt nanoelectrodes: Evidence of surface diffusion and spillover. *J. Am. Chem. Soc.* **2009**, *131*, 14756−14760.
(41) Flanagan, T. B.; Oates, W. A. The palladium-hydrogen system. *Annu. Rev. Mater. Sci.* **1991**, *21*, 269−304.
(42) Zoltowski, P.; Makowska, E. Diffusion coefficient of hydrogen in α-phase palladium and palladium-platinum alloy. *Phys. Chem. Chem. Phys.* **2001**, *3*, 2935−2942.
(43) Knapton, A. G. Palladium alloys for hydrogen diffusion membranes. *Platinum Met. Rev.* **1977**, *21*, 44−50.
(44) Bard, A. J.; Faulkner, L. R.; Leddy, J.; Zoski, C. G. *Electrochemical Methods: Fundamentals and Applications*; Wiley: New York, 1980; Vol. 2.

DOI: 10.1021/acs.jpcc.8b03770
J. Phys. Chem. C 2018, 122, 15421−15426